




Response of fuzzy clustering on different threshold determination algorithms in spectral change vector analysis over Western Himalaya, India

SINGH Sartajvir^{1*}  <http://orcid.org/0000-0002-4451-4949>;  e-mail: sartajvir.singh@chitkarauniversity.com

TALWAR Rajneesh²  <http://orcid.org/orcid/0000-0002-2109-8858>; e-mail: rtphdguidance@gmail.com

* Corresponding author

¹ Department of Electronics and Communication Engineering, Chitkara University, Himachal Pradesh, 174 103, India

² Chandigarh Group of Colleges, Technical Campus, Jhanjeri 140 307, India

Citation: Singh S, Talwar R (2017) Response of fuzzy clustering on different threshold determination algorithms in spectral change vector analysis over Western Himalaya, India. Journal of Mountain Science 14(7). DOI: 10.1007/s11629-016-4248-0

© Science Press and Institute of Mountain Hazards and Environment, CAS and Springer-Verlag Berlin Heidelberg 2017

Abstract: Change detection is a standard tool to extract and analyze the earth's surface features from remotely sensed data. Among the different change detection techniques, change vector analysis (CVA) have an exceptional advantage of discriminating change in terms of change magnitude and vector direction from multispectral bands. The estimation of precise threshold is one of the most crucial task in CVA to separate the change pixels from unchanged pixels because overall assessment of change detection method is highly dependent on selected threshold value. In recent years, integration of fuzzy clustering and remotely sensed data have become appropriate and realistic choice for change detection applications. The novelty of the proposed model lies within use of fuzzy maximum likelihood classification (FMLC) as fuzzy clustering in CVA. The FMLC based CVA is implemented using diverse threshold determination algorithms such as double-window flexible pace search (DFPS), interactive trial and error (T&E), and 3×3-pixel kernel window (PKW). Unlike existing CVA techniques, addition of fuzzy clustering in CVA permits each pixel to have multiple class categories and offers ease in threshold determination process. In present work, the comparative analysis has highlighted the performance of FMLC based CVA over

improved SCVA both in terms of accuracy assessment and operational complexity. Among all the examined threshold searching algorithms, FMLC based CVA using DFPS algorithm is found to be the most efficient method.

Keywords: Change vector analysis (CVA); Fuzzy maximum likelihood classification (FMLC); Double-window flexible pace search (DFPS); Interactive trial and error (T&E); Pixel kernel window (PKW)

Introduction

Change detection analysis plays a significant role in observing land use and land cover (LULC) earth surface variations with the help of remotely sensed multispectral imagery. Since past few decades, different change detection techniques have been developed and summarized for qualitative as well as quantitative measurement of spatial variations over multi-temporal scale (Lu et al. 2004; Singh & Talwar 2014). Amongst various algorithms, a conceptual extension of image differencing, termed as change vector analysis (CVA) algorithm is preferred due to existence of unique advantage of describing change

Received: 13 October 2016
Revised: 16 January 2017
Accepted: 19 April 2017

in terms of both change magnitude and vector direction (Malila 1980). CVA algorithm is found to be more appropriate under different conditions encountered in diverse range of change detection applications (Michalek et al. 1993; Allen and Kupfer 2000; Silva et al. 2003). Since past few decades, a series of developments has been made in CVA such as improved CVA (ICVA), CVA in posterior probability space, CVA using cross correlogram spectral matching (CCSM), median CVA (MCVA) and robust CVA (RCVA) (Allen and Kupfer 2000; Chen et al. 2003; Chen et al. 2011; He et al. 2013; Varshney et al. 2012; Thonfeld et al. 2016). The efficacy of different CVA based change detection techniques has already been tested over mountainous region by various authors (Sharma et al. 2013; Singh & Talwar 2015a).

As far as threshold selection is concerned, a number of threshold determination algorithms have been designed and implemented over CVA. Initially, choice of threshold was generally achieved by using manual empirical approaches based on training samples (Allen and Kupfer 2000). Latterly, double-window flexible pace search (DFPS), interactive trial and error (T&E) procedure based on mean and standard deviation were developed to compute a potential threshold value (Chen et al. 2003; Fung and LeDrew 1988; He et al. 2013). They may require number of iterations to be performed over training sample by varying adjustment coefficient. Kontoes (2008) has proposed threshold algorithm based on 3×3-pixel kernel window (PKW) to compute the change magnitude between any pixel (date-1) and the corresponding nine pixels positioned in the neighborhood (date-2). Varshney et al. (2012) have modified 3×3 PKW by introducing concept of discriminating change on the basis of standard deviation and mean. From practical consideration, no one threshold algorithm is fully autonomous, accurate and applicable in all circumstances. Each threshold algorithm has their own advantages as well as disadvantages and developed for specific application. The threshold searching algorithm should be effective, permits ease in its implementation, less dependent on user, less time consuming and robust against diverse magnitude values. Previous literature shows the comparison between diverse CVA based change detection algorithms and their associated threshold detection

algorithms over mountainous region (Singh and Talwar 2015a, b). A summarization of existing threshold algorithms developed or implemented on CVA using different satellite sensors has been shown in Table 1.

Another problem associated with CVA technique is the detection of pixels which falls under multiple class categories, termed as mixed pixels. The existence of mixed pixels depends upon pixel-width which may not be adequate enough to capture the fine details of earth parameters especially in case of mountainous region. Due to the presence of mixed pixels, it may be difficult to identify the exact category of pixels during change discrimination procedure and in results, downfall can be seen in accuracy assessment. Therefore, it is essential to separate mixed pixels before proceeding for further analysis. Keeping in mind these considerations, this research comes out with a methodology based on the capabilities of CVA in extraction of change and flexibilities of fuzzy clustering techniques. Fuzzy logic is an effective tool to identify association of each pixel with respect to concerned features by assigning membership of belongingness (Zhang and Foody 1998; Singh and Talwar 2016). It has also been observed that fuzzy based classification is only a possible solution to characterize a pixel value based on their percentage of belongingness to specified classes (Foody and Atkinson 2002).

The present study adopts a fuzzy approach to overcome existing problems in CVA with the use of fuzzy maximum likelihood classification (FMLC). This model has two advantages: (1) fuzzy as soft classification permits each pixel to have multiple or partial change categories and allows the extraction of mixed pixel information and (2) ease in selection of threshold value from limited range of change magnitude values present in fuzzy classified imagery. The main focus of this research is to study the response of fuzzy clustering on different threshold algorithms over mountainous region. From this perspective, the impact of FMLC based CVA (with fuzzy clustering) has been analyzed over well-accepted and commonly-used threshold searching models (DFPS, T&E and 3×3 PKW). Apart from its validations, the outcomes of FMLC based CVA are compared with improved SCVA (without fuzzy clustering) using same threshold algorithms.

Table 1 A comparison between different threshold algorithms implemented over CVA as change detection techniques

Algorithms	Characteristics	Merits	Demerits	Data and study area
Double-window flexible pace search (DFPS)	1. Require two windows (internal & external) and search parameter to compute threshold (T_V). 2. Upper (U_L) and lower limits (L_L) provided to search T_V within a specified range.	1. Less dependent on user experience (Require user knowledge only in sample selection phase). 2. Search can be performed within specified limit and at any decimal points.	1. Consume more time if the training sample doesn't meet predefined criteria. 2. Sometime unable to fulfill criteria.	MODIS over mountainous region (Singh and Talwar 2015b, 2016); TM over LULC (Chen et al. 2003); AWiFS over rugged terrain (Sharma et al. 2012)
3×3-pixel kernel window (PKW)	1. Considered pixel's geographic neighborhood as 3×3-PKW 2. Require a reference pixel along with 3×3-pixel window.	1. Overcome the problem of erroneously identified as 'change' pixels from neighboring pixels.	1. It is difficult to cover all pixels in window. 2. Requirement of user confidence as decision making tool.	Landsat TM/ ETM+ over fragmented landscape (Kontoes 2008)
Interactive Trial and error (T&E)	1. Based on standard deviation (σ), mean (μ). 2. In addition, an adjustment factor (λ) is involved.	1. Avoid the situation where erroneously pixels are identified due to spatial resolution. 2. Avoid error due to misclassification.	1. Consume more time. 2. At each step of λ , threshold need to be computed.	MODIS over mountainous region (Singh and Talwar 2015b); MODIS using VI (Chunyang et al. 2013)
3×3 PKW based on standard deviation & mean	1. Selection of threshold based on standard deviation (σ), mean (μ) and 3×3 window.	1. Add the merits of both 3×3 kernel and T&E technique.	1. Requirement of user knowledge to identify sample and vary adjustment factor (λ).	Landsat TM/ ETM+ over LULC (Varshney et al. 2012)
Inverse triangular function (ITF)	1. The standard deviation (σ), mean (μ) of each principal component of difference image is calculated.	1. Takes care of the redundant information in the given bands. 2. Avoid the misclassification of pixels due to spatial resolution.	1. Limited applicability of ITF algorithm.	LISS-III over LULC (Baisantry et al. 2012)
Empirical procedures	1. Selection of threshold on the basis of reference data.	1. less complexity. 2. Require limited parameters to compute T_V .	1. Requirement of analyst's expert knowledge about the study area.	MODIS over western Himalaya (Singh and Talwar 2015b); TM (Nackaerts et al. 2005)
Otsu thresholding	1. Minimize the intra-class variance and maximize the inter-class variance of distributions of bimodal histograms.	1. Robust against large range magnitude values.	1. Less sensitive against extensive variation of global distributions of object.	RapidEye and Kompsat-2 over LULC (Thonfeld et al. 2016)

Notes: TM: Thematic Mapper; ETM+: Enhanced Thematic Mapper Plus; AWiFS: Advance Wide Field Sensor; MODIS: Moderate Resolution Imaging Spectroradiometer; LISS: Linear Imaging Self-Scanning Sensors; LULC: Land use and land cover; VI: Vegetation Index.

1 Study Area and Dataset

The present study area, shown in Figure 1, is situated in the lower zone of western Himalaya, Lahul, Himachal Pradesh, India. The geographical location lies between latitudes 32°12' – 33°24' N and longitudes 76°38' – 77°73' E. This region is characterized by very low temperatures and heavy snowfall. The MODIS dataset has been used in present work that have sufficient dynamic range and spectral coverage to measure the reflected energy from the Earth's surface in 36 spectral narrow bands (0.405µm to 14.385µm) with wide scanning swath width of 2330 km. A digital elevation model (DEM) of corresponding area is obtained from Advanced Space borne Thermal Emission and Reflection Radiometer (ASTER) to generate illumination image, slope and aspect maps of corresponding study site. The slope value varies from 1° to 85° with an average of 26° and aspect value varies from 0° to 360° with mean aspect equals to 182°. The elevation ranges stretched from 2377 m to 6576 m above mean sea level (AMSL) with an average of 4270 m AMSL.

2 Methodology

Preliminary processing (geometric, radiometric and topographic corrections) are essential to be performed on digital number (DN) imagery to generate reflectance imagery before any further considerations. The geometric correction was performed using 50 ground control points (GCP) with second order polynomial transformation to preserve root mean square error (RMSE) less than one (Mather 2004). The spectral reflectance R' from the sensor radiance is implemented as follow (Mishra et al. 2009b; Sharma et al. 2013):

$$R' = \frac{\pi L_{\lambda} d_{ES}^2}{A_0 \cos \theta_z} \quad (1)$$

where θ_z is solar zenith angle between sun rays and zenith direction; d_{ES} is distance between earth and sun; L_{λ} is the corrected spectral radiance; A_0 is the mean solar exo-atmospheric spectral irradiance of MODIS bands (Mishra et al. 2009b). Afterwards, slope match technique as topographic correction was implemented over reflectance imagery to overcome the effects of different illumination that

existed due to rugged topography of Himalaya (Nichole 2006). The topographic correction is selected on the basis of comparative analysis performed over mountainous region by various authors (Mishra et al. 2009a; Singh et al. 2011). The slope match topographic correction S'_m is computed as follow:

$$S'_m = \left\{ [R' + (R'_{max} - R'_{min})] \times \left(\frac{\cos i_{sa} - \cos i}{\cos i_{sa}} \right) \times \left[\frac{(S_a^1 - N_a)}{(N_a^1 - N_a)} \right] \right\} \quad (2)$$

where R' is the reflectance imagery; R'_{max} and R'_{min} are the maximum and minimum spectral reflectance values, respectively; $\cos i$ and $\cos i_{sa}$ are scaled (0-255) illumination imagery and scaled (0-255) sun-facing illuminated slopes instead of overall mean, respectively; The N_a and N_a^1 are north-aspect and north-aspect after first stage normalization, respectively; and S_a^1 is south-aspect after first stage normalization. Figure 2a and 2b are represented the topographically corrected reflectance imagery of date-1 and date-2, respectively. The overall methodology of proposed work is divided into four parts: (a) fuzzy logic; (b) change magnitude; (c) threshold determination and (d) change direction.

2.1 Fuzzy based maximum likelihood classification (MLC)

The fuzzy based MLC is implemented over topographically corrected imagery to quantify the pixels which are allocated to more than one class category with certain degree of belonging (Foody 2002). Contrarily, conventional methods are based on hard classification in which a pixel is dedicatedly assigned to one category only. Sometimes, the crisp values between the change and no-change boundaries may not be accurately visualized and in results, affect the accuracy. To overcome such problems, fuzzy logic delivers a realistic solution to identify the overlapped clusters (Mishra et al. 2012). Over selected study site, there may be the possibility of a pixel to lie within two or more class categories with certain degree of belongingness. Therefore, deriving a fuzzy classification is essential for such pixels to describe the change as a degree of intensely associated with their equivalent class category as follow (Melesse and Jordon 2002):

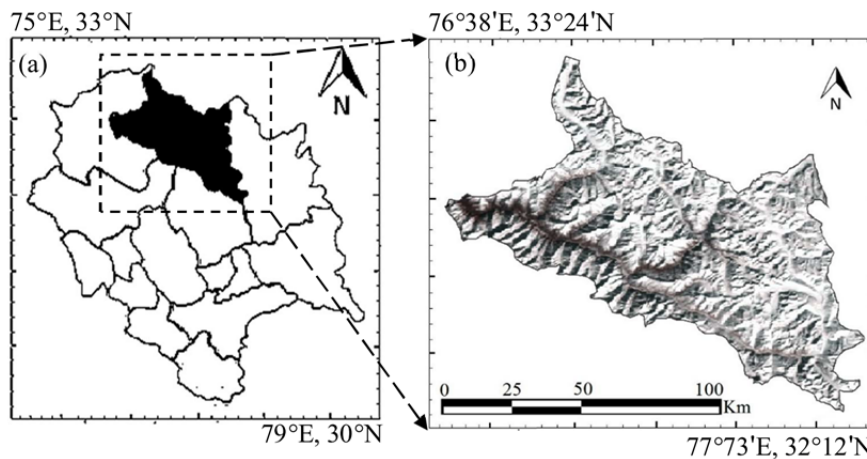


Figure 1 Study location (a) Lahul, Himachal Pradesh, India (b) MODIS sensor satellite imagery.

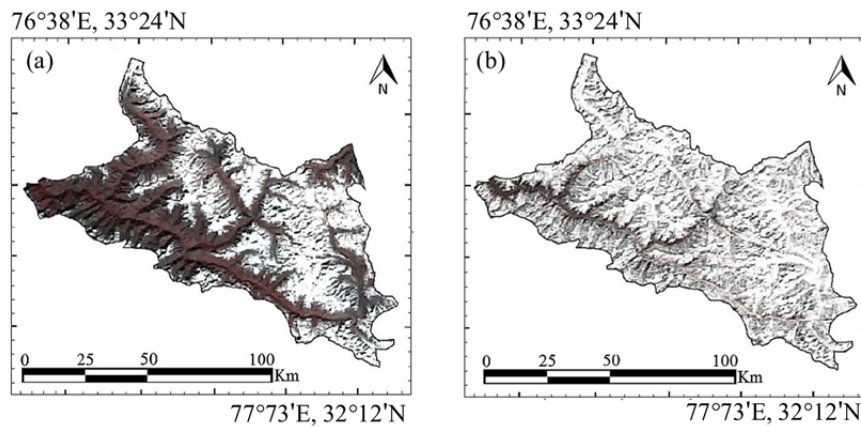


Figure 2 Topographically corrected (a) date-1 (Pre) imagery (b) date-2 (Post) imagery.

$$F(j) = \sum_{w=0}^t \sum_{x=0}^t \sum_{y=0}^l \frac{W_{wx}}{D_{wxy}(j)} \quad (3)$$

where $F(j)$ is the total weighted distance of window for j th class, w is a row index of window, x is a column index of window, y is layer index of fuzzy set, t is size of window, l is number of fuzzy layers considered, $D_{wxy}(j)$ is distance file for j th class, and W_{wx} is weight table for window. The convolution of fuzzy generates a layer classified imagery by computing the total weighted inverse distance. Further, it allocates midpoint pixel in the class category with the largest total inverse distance summed over the whole set of fuzzy classified layers (ERDAS 1999).

2.2 Change vector analysis (CVA)

CVA is a multivariate technique which accepts an array of spectral bands and distinguishes the changes in two primary components: (a) vector direction; and (b) change magnitude (Malila 1980).

CVA offers various advantages over exiting algorithms such as: (a) processing number of spectral bands simultaneously; (b) relaxation from spatial spectral errors generally inherent in multi-temporal classification; and (c) detection of changes in different terrain types and conditions (Johnson and Kasischke 1998). The overall operation of CVA is divided into three portions: (a) determination of change magnitude using Euclidean distance between vector end points in spectral space, (b) choice of optimum threshold value based on manual or semiautomatic procedures and (c) identify the change vector direction based on cosine direction to categorize the change. The change magnitude $|\vec{H}|$ is computed on the basis of Euclidean distance from fuzzy classified imagery as follow:

$$\vec{H} = \begin{Bmatrix} (y_1 - y_2)_1 \\ (y_1 - y_2)_2 \\ \dots \\ (y_1 - y_2)_n \end{Bmatrix} = \begin{Bmatrix} y_{n1} \\ y_{n2} \\ \dots \\ y_{nn} \end{Bmatrix} \quad (4)$$

$$|\vec{H}| = [\sum_i^n (y_{hi})^2]^{1/2} \tag{5}$$

where y_1 and y_2 represent the pixel values of date-1 and date-2 imagery, respectively, y_{hi} represents difference of two multi-temporal pixels located at same geographic coordinates and n is total number of spectral bands in imagery.

Figure 3a and 3b have been represented change magnitude imagery computed from improved SCVA and FMLC based CVA, respectively. In magnitude imagery, brighter or higher value of a pixel represents maximum change while darker region or low value of a pixel represents minimum change in spectral space.

2.3 Threshold Algorithms

Once the change magnitude imagery is computed, change and no-change information can be extracted from it using threshold determination algorithm. Threshold procedure is necessary to be implemented on change magnitude imagery because unchanged pixel falls within a category of change pixels due to existence of some factors such as improper normalization and noise (Johnson and Kasischke 1998). The threshold procedures are become much more complicated when more than two spectral bands are involved. To study the response of different threshold algorithms over FMLC based CVA, well developed models such as interactive T&E measures (He et al. 2013), DFPS (Chen et al. 2003) and 3×3 PKW threshold (Kontoes 2008) algorithms are implemented in this study.

2.3.1 Double-window flexible pace search (DFPS)

Chen et al. (2003) proposed DFPS threshold algorithm acted as a semiautomatic process that requires certain degree of image analyst’s skill set.

In this algorithm, the initial step is to select a sample from magnitude imagery based on predefined parameters such: (a) sample must covered all possible types of changes; (b) it must include only change pixels; and (c) avoid the extreme low values of magnitude imagery. However, it is observed that under some conditions, it is not possible to cover all types of change categories in a sample and hence, multiple samples are required to be analyzed. FMLC based CVA overcomes same problem up to a great extent by selecting a sample based on visual interpretation which comprises maximum fuzzy change classes or layer index. In layer index, a pixel containing maximum fuzzy layers is represented by higher value of change magnitude while in case of minimum fuzzy layers, corresponding pixel is represented by lower value of change magnitude (Figure 3b). The DFPS algorithm has been implemented over change magnitude imagery to discriminate the change and unchanged (Figure 4a).

Steps to execute the DFPS algorithm:

1) Select the training samples based on aforementioned criteria from change magnitude imagery.

2) Separate the sample into two parts: (a) outer window and (b) inner window from improved SCVA (Figure 5a) and FMLC based CVA (Figure 5b).

3) Set lower limit (L_L) and upper limit (U_L) manually within a range from minimum to maximum value of change magnitude and specify the step size (S_s) based on user confidence (λ) as follow:

$$S_s = \frac{U_L - L_L}{\lambda} \tag{6}$$

4) At each step of nominated threshold value (T_V), achievement rate (A_R) of corresponding

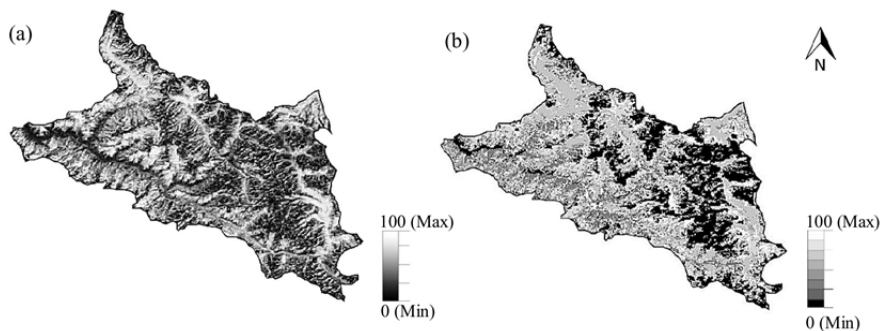


Figure 3 Change magnitude imageries from (a) improved SCVA (b) FMLC based CVA.

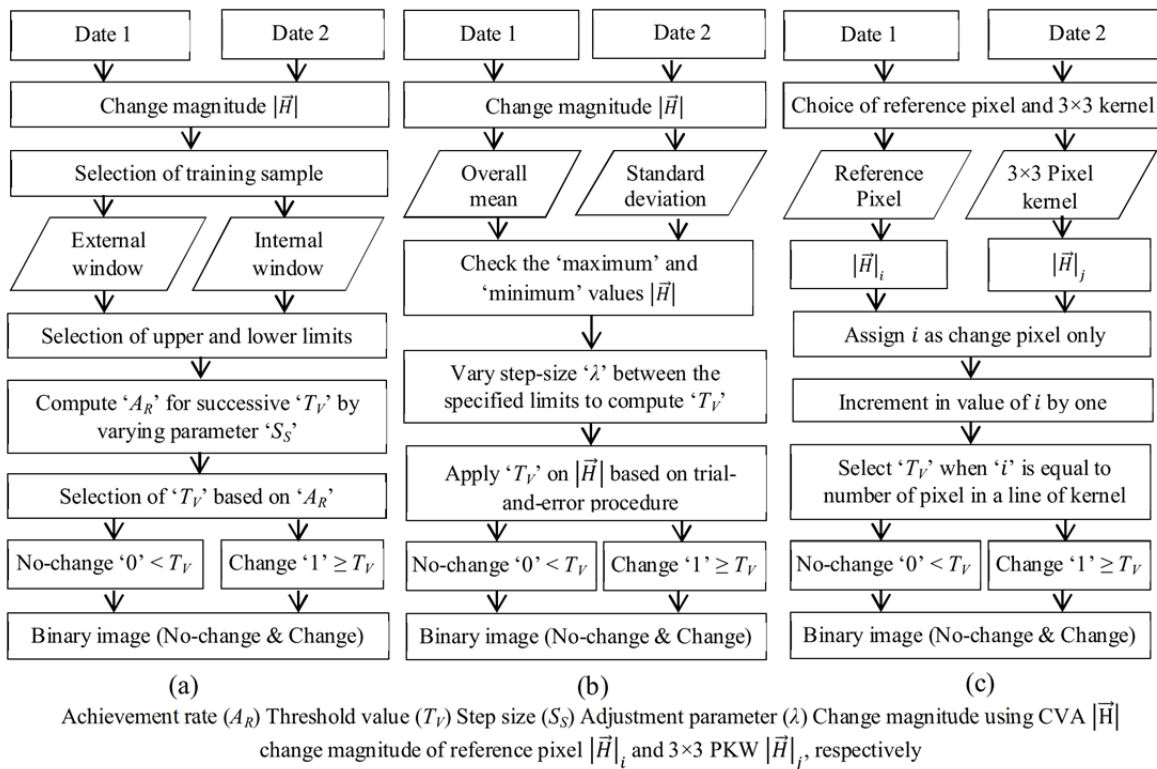


Figure 4 Comparison of CVA based threshold determination algorithms applied on fuzzy classified imageries (a) DFPS technique (b) T&E technique (c) 3×3 PKW technique.

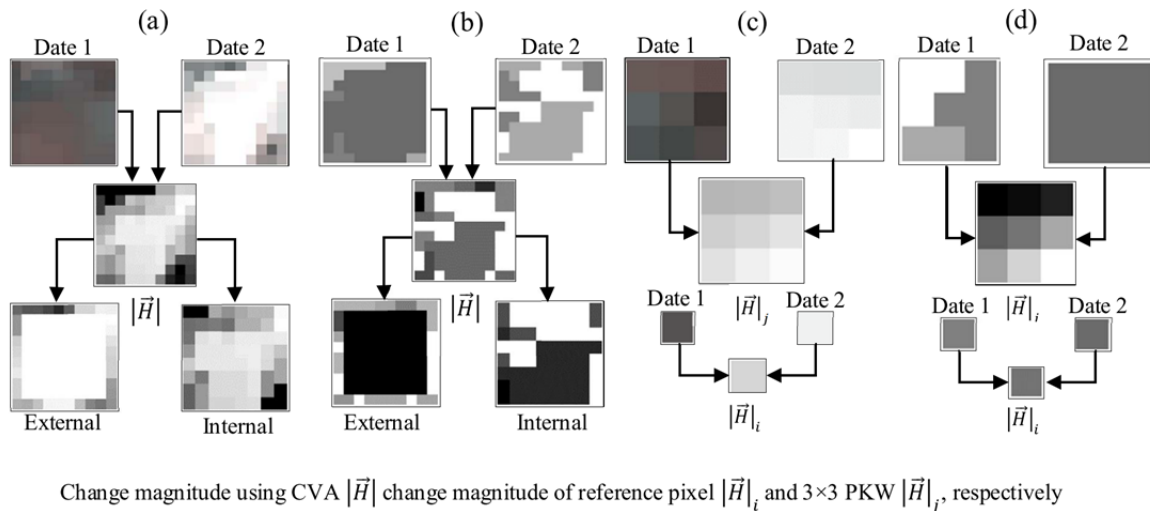


Figure 5 Selected of training sample from (a) DFPS algorithm with improved SCVA (b) DFPS algorithm with FMLC based CVA (c) 3×3 PKW with improved SCVA (d) 3×3 PKW with FMLC based CVA.

(T_V) is computed as follow:

$$A_R(\%) = \frac{(I_c - E_c)}{I_t} \quad (7)$$

where I_c and E_c represented number of change pixels occurred in internal window and external window, respectively and I_t is the total number pixels inside the internal training window.

1) Increase the step size (S_S) up to required decimal points within the specified ranges of (L_L) and (U_L) as shown in Table 2.

2) When highest A_R is achieved, stop the iteration and apply specific T_V to change magnitude imagery to generate binary imagery ('1' value to represent change and '0' value to represent no-change).

Table 2 and 3 shown the results of selected threshold value based on achievement rate using DFPS algorithm on FMLC based CVA and improved SCVA, respectively. Figure 6a and 6d represented the binary imagery generated from FMLC based CVA and improved SCVA, respectively.

2.3.2 Interactive Trial and Error (T&E)

The T&E procedure introduced by Fung and Ledrew (1988) in which a series of threshold values are considered on the basis of standard deviation (σ) and mean (μ) to discriminate the change pixels from unchanged pixels. A set of training samples are required to be selected and they must also include all types of change categories available in imagery. In order to formulate interactive T&E, three parameters, entitled as standard deviation (σ), mean (μ) and adjustment coefficient (λ) are computed from training samples (He et al. 2013). The value of adjustment coefficient can be initiated from 0.1 until the maximum value of threshold reaches to the maximum value change magnitude. The T&E algorithm has been implemented over fuzzy classified magnitude imagery as shown in Figure 4b.

Steps to execute T&E algorithm

1) Select a set of training samples to cover all types of change categories available in selected study site.

2) Extract the values of standard deviation (σ) and overall mean (μ) from nominated training samples.

3) Initially, set the adjustment parameter (λ) at value 0.1 and implement as follow:

$$T_V = \mu + (\lambda \times \sigma) \tag{8}$$

4) In subsequent iterations, the value of λ is increased at each step by 0.1 on the basis of user confidence and continue the iteration until the T_V reaches to its maximum value.

5) At each step, binary (change and no-change) imagery is computed for specific T_V and compared with reference imagery to build an error matrix.

6) At last, potential threshold correspond to maximum kappa coefficient is assigned to change magnitude imagery.

Figure 6b and 6e represented the binary imagery generated from FMLC based CVA and improved SCVA, respectively.

2.3.3 3×3-pixel kernel window (PKW)

Kontoes (2008) has proposed 3×3-PKW algorithm to overcome the problem of overestimation because it is observed that spectral properties of the no-change pixels are effected by the neighboring change pixels. In this algorithm, Euclidean distance is computed between a reference pixel on date-1 imagery and

Table 2 Results of selection of threshold value based on achievement rate in DFPS thresholding algorithm with FMLC based CVA

$U_L=80, L_L=20$ $S_S=20$		$U_L=60, L_L=20$ $S_S=10$		$U_L=55, L_L=35$ $S_S=5$		$U_L=49, L_L=45$ $S_S=1$		$U_L=46.5, L_L=46.1$ $S_S=0.1$		$U_L=46.29, L_L=46.25$ $S_S=0.01$	
T_V	A_R (%)	T_V	A_R (%)	T_V	A_R (%)	T_V	A_R (%)	T_V	A_R (%)	T_V	A_R (%)
20	15.61	20	15.61	35	46.47	45	46.47	46.1	46.47	46.25	46.47
40	46.47	30	46.47	40	46.47	46	46.47	46.2	46.47	46.26	46.47
60	18.75	40	46.47	45	46.47	47	50	46.3	50	46.27	46.47
80	18.75	50	50	50	50	48	50	46.4	50	46.28	46.47
--	--	60	18.75	55	50	49	50	46.5	50	46.29	50

Table 3 Results of selection of threshold value based on achievement rate in DFPS thresholding algorithm with improved SCVA

$U_L=80, L_L=20$ $S_S=20$		$U_L=70, L_L=30$ $S_S=10$		$U_L=65, L_L=50$ $S_S=5$		$U_L=64, L_L=56$ $S_S=2$		$U_L=46.5, L_L=46.1$ $S_S=0.1$		$U_L=46.29, L_L=46.25$ $S_S=0.01$	
T_V	A_R (%)	T_V	A_R (%)	T_V	A_R (%)	T_V	A_R (%)	T_V	A_R (%)	T_V	A_R (%)
20	46.87	30	50	50	59.37	56	59.37	59.1	59.37	59.26	59.37
40	54.83	40	54.83	55	59.37	58	59.37	59.2	59.37	59.27	59.37
60	59.37	50	59.37	60	64	60	60.93	59.3	60.93	59.28	59.37
80	28.12	60	64	65	46.87	62	53.12	59.4	60.93	59.29	59.37
--	--	70	28.12	--	--	64	51.56	59.5	60.93	59.30	60.93

Notes: U_L , Upper limit; L_L , lower limit; S_S , Step size; T_V , threshold value; A_R , achievement rate.

corresponding 3×3-pixel window situated in the immediate neighborhood of predefined pixel on date-2 imagery. Moreover, a coefficient is required to be computed based on user confidence that is related to the number of no-change pixels occurred. Varshney et al. (2012) suggested another enhancement in which threshold value is evaluated on the basis of mean (μ) and standard deviation (σ) of specified pixel, and (3×3) kernel window. The 3×3-PKW algorithm has been implemented on fuzzy classified magnitude imagery as shown in Figure 4c.

Steps to execute 3×3-PKW algorithm

1) Select a reference pixel representing only change area from date-1 and on the other end, select a corresponding kernel window of 3×3-pixel size from date-2 as shown in Figure 5c and 5d for SCVA and FMLC based CVA, respectively.

2) Compute the change magnitude of reference pixel as well as 3×3 PKW.

3) Identify the standard deviation (σ) as well as mean (μ) from reference pixel and 3×3-pixel kernel window magnitudes.

4) Compute the threshold value (T_V) according to Eq.(8) and adjustment factor (λ) is computed based on user confidence.

5) Check the number of pixels detected inside the window: if it is more than five, then the

threshold value (T_V) can be used to generate binary image otherwise the value of reference pixel can be increased and repeat the first five steps.

6) When the aforementioned criteria (step 5) is achieved, then the pixels in change magnitude imagery having value more than threshold value T_V can be replaced with the change and rest of the pixels are remain unchanged.

Figure 6c and 6f represented the binary imagery generated from FMLC based CVA and improved SCVA, respectively.

2.4 Change vector direction

In order to determine ‘from-to’ change, change vector direction can be computed in different ways such as cosine based (Chen et al. 2003), direction in the polar domain (Allen and Kupfer 2000), principal component analysis (PCA) in the multi-temporal domain (Lambin and Strahler 1994), positive and negative shifts in spectral space (Nackaerts et al. 2005) and sector coding based change category (Malila 1980). The direction cosines technique based on cosine angles is implemented as an angle function that lies between change vector and individual spectral response to recognize the different change categories. The change direction (θ) may also be identified as

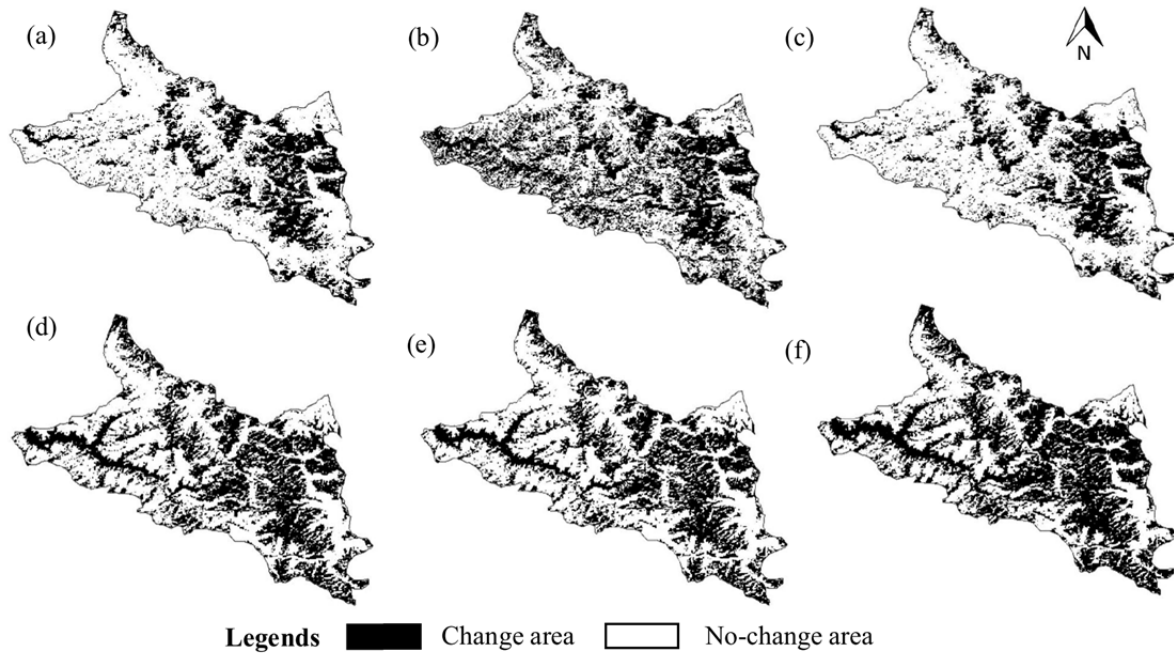


Figure 6 CVA based binary (Change and no-change) imageries computed from (a) DFPS with FMLC based CVA (b) T&E with FMLC based CVA (c) 3×3 PKW with FMLC based CVA (d) DFPS with improved SCVA (e) T&E with improved SCVA (f) 3×3 PKW with improved SCVA.

vectors $\vec{H} = (Cos \theta_1, Cos \theta_2, \dots, Cos \theta_i)$ and direction angles $(\theta_1, \theta_2, \dots, \theta_i)$, respectively.

$$\theta^i = Cos^{-1}\left(\frac{y_{hi}}{|\vec{H}|}\right) \quad (9)$$

where y_{hi} represents difference of two multi-temporal pixels located at same geographic coordinates.

Afterwards, the cosine direction in terms of change vector are stacked together to generate a multidimensional change direction imagery. Minimum-distance classification is considered to discriminate the category of change because their features and categories are already identified. Moreover, similarity measure is used as a distance measure between distributed functions in Minimum-distance classification (Varshney et al. 2012). Figure 7 represented the change map imagery computed from FMLC based CVA and improved SCVA using different threshold algorithms.

3 Results and Discussions

3.1 Visual interpretation and accuracy assessment

Figures 6a to 6c are representing the change and no-change imagery generated from three threshold algorithms (DFPS, T&E and 3×3 PKW) implemented over FMLC based CVA and on Figures 6d to 6e are representing change and no-change imagery generated from same algorithms implemented over improved SCVA. White and black tones in the resultant images (Figure 6) indicate change and no-change pixels, respectively in the region. These images are assessed with the help of error-matrix as standard assessment tool that includes various parameters such as overall accuracy (OA) to represent correctness of change map, commission error (CE) to identify erroneously included pixel into different category, kappa coefficient (Kc) that convey the accuracy of classification after adjustment for chance, producer accuracy (PA) and user accuracy (UA) representing individual class-category accuracies. Table 4 and 5 represent the results of error matrixes generated from change/no-change mask imagery computed from different threshold determination techniques (DFPS, T&E and 3×3 PKW).

The DFPS algorithm using FMLC based CVA achieved highest accuracy in OA (89.45%), PA (90.4% in change and 88.55% in no-change category), UA (88.28% in change and 90.63% in no-change category), overall Kc (0.78) and least CE ranges from 9.3% to 11.71% as compare to other threshold algorithms. Whereas DFPS algorithm using improved SCVA also achieved highest accuracy in OA (88.28%), PA (85% in change and 92.24% in no-change category), UA (92.97% in change and 83.59% in no-change category), overall Kc (0.76) and least CE ranges from 7% to 16.04% as compare to other threshold algorithms. On the other hand, category change maps from FMLC based CVA and improved SCVA are shown in Figures 7a to 7c and Figures 7d to 7e, respectively for different threshold algorithms (DFPS, T&E and 3×3 PKW). Table 6 represents the results of accuracy assessment generated from change category maps computed from FMLC based CVA and improved SCVA for different threshold algorithms (DFPS, T&E and 3×3 PKW). The DFPS algorithm using FMLC based CVA achieved highest accuracy (OA=88.28% as compare to other studies. According to visual interpretation and accuracy procedures, very less difference is observed between change and no-change mask imagery from DFPS and 3×3 kernel window while T&E change mask shown much difference than other algorithms in both FMLC based CVA and improved SCVA techniques. According to the accuracy assessment, DFPS performed well enough in case of both FMLC based CVA and improved SCVA but better accuracy achieved from FMLC based CVA.

3.2 Relative performance of FMLC based CVA and improved SCVA over different threshold algorithms

To prevent any bias caused by threshold algorithm, FMLC based CVA and improved SCVA are implemented using three different threshold algorithms: (a) DFPS, (b) T&E and (c) 3×3 PKW. A comparison analysis based on visual interpretation and accuracy assessment has represented a noticeable difference between FMLC based CVA and improved SCVA. In details, DFPS and 3×3 PKW represented that overall distribution of change and no-change pixels are similar in visual and accuracy results while in case of T&E, the

Table 4 Error-matrixes for assessing the threshold value using different threshold determination techniques

Techniques	Classified data (Feb-2011)	Reference data (Nov-2010)			Commission error (%)
		Change	No-change	Column total	
DFPS with FMLC based CVA	Change	113	15	128	11.71
	No-change	12	116	128	9.3
	Row total	125	131	256	
	Commission error (%)	9.6	11.45		
	Overall accuracy = 89.45%, Kappa coefficient = 0.7891				
T&E with FMLC based CVA	Change	112	16	128	12.5
	No-change	25	103	128	19.5
	Row total	137	119	256	
	Commission error (%)	18.2	13.44		
	Overall accuracy = 83.98%, Kappa coefficient = 0.6797				
3×3 PKW with FMLC based CVA	Change	119	9	128	7.03
	No-change	21	107	128	16.40
	Row total	140	116	256	
	Commission error (%)	15	7.75		
	Overall accuracy = 88.28%, Kappa coefficient = 0.7656				
DFPS with improved SCVA	Change	111	17	128	13.2
	No-change	13	115	128	10.15
	Row total	124	132	256	
	Commission error (%)	10.48	12.87		
	Overall accuracy = 88.28%, Kappa coefficient = 0.7656				
Trial & Error with improved SCVA	Change	110	18	128	14.06
	No-change	21	107	128	16.4
	Row total	131	125	256	
	Commission error (%)	16.03	14.4		
	Overall accuracy = 84.77%, Kappa coefficient = 0.6953				
3×3 PKW with improved SCVA	Change	111	17	128	13.28
	No-change	24	104	128	18.75
	Row total	135	121		
	Commission error (%)	17.77	14.04	256	
	Overall accuracy = 83.98%, Kappa coefficient = 0.6797				

Table 5 Results of error matrixes generated from change and no-change imageries of different threshold determination techniques

Threshold determination techniques	Change			No-change			Overall Assessment			
	PA (%)	UA (%)	Kc	PA (%)	UA (%)	Kc	OA (%)	Kc	CE _{min} (%)	CE _{max} (%)
DFPS with FMLC based CVA	90.4	88.28	0.77	88.55	90.63	0.8	89.45	0.78	9.3	11.71
T&E with FMLC based CVA	82.22	86.72	0.71	85.95	81.25	0.64	83.98	0.67	13.28	18.75
3×3 PKW with FMLC based CVA	89.52	86.72	0.74	87.12	89.84	0.79	88.28	0.76	10.15	13.2
DFPS with improved SCVA	85	92.97	0.84	92.24	83.59	0.70	88.28	0.76	7.0	16.04
Trial & Error with improved SCVA	83.97	85.94	0.71	85.6	83.59	0.67	84.77	0.69	14.06	16.03
3×3 PKW with improved SCVA	81.75	87.50	0.73	86.5	80.47	0.63	83.98	0.67	12.5	19.5

distribution of change pixels is not up to an extent. The reasons behind the existence of such results are due to the lower threshold value detected in DFPS and 3×3 PKW algorithm whereas in case T&E algorithm, higher threshold value detected. In

change category map, imagery computed from DFPS algorithms are represented better accuracy in both of FMLC based CVA (OA=88.28%, Kc=0.78) and improved SCVA (OA=85.16%, Kc=0.74) with respect to other algorithms.

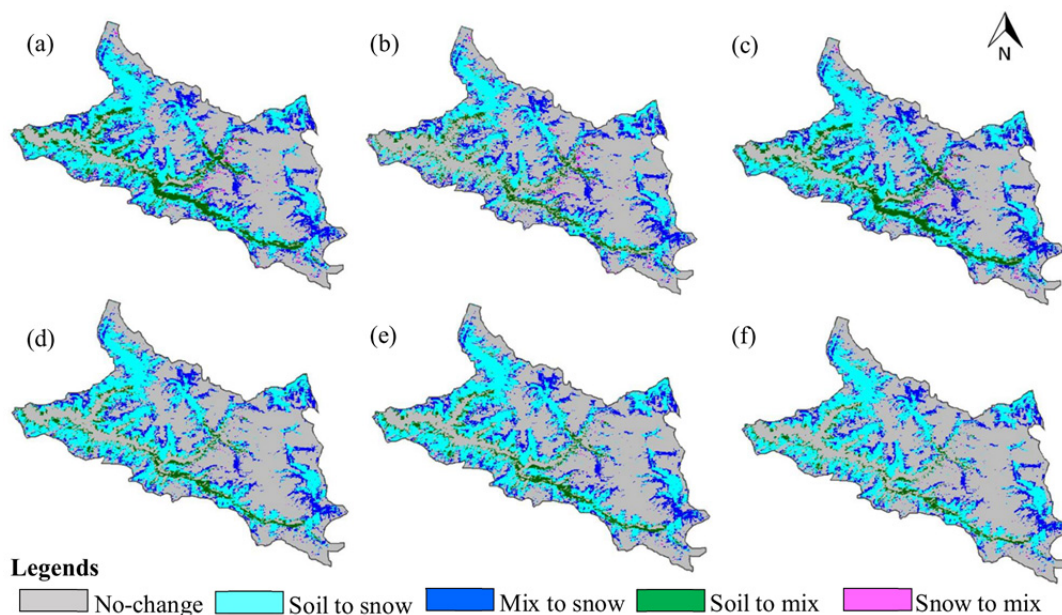


Figure 7 CVA based change map imageries computed from (a) DFPS with FMLC based CVA (b) T&E with FMLC based CVA (c) 3×3 PKW with FMLC based CVA (d) DFPS with improved SCVA (e) T&E with improved SCVA (f) 3×3 PKW with improved SCVA.

It is inferred that FMLC based CVA using DFPS algorithms performed very well both in qualitative and quantitative analysis as compare to improved SCVA. Note that, FMLC based CVA generates change magnitude imagery having limited number of magnitude range and such limited range helps the user to easily identify the all types of changes in the training sample. This simplicity makes the threshold algorithm more efficient and delivers ease in obtaining training errors and maximum accuracy.

3.3 Conclusions

In this study, FMLC based CVA technique has been developed in order to consider mixed pixels unlike wise in existing CVA based algorithm, a change pixel is assigned to a specific class only. For theoretical and practical reflections, the integration of fuzzy in CVA is more suitable and realistic towards situations where overlapping clusters are existed. For any change detection technique, accuracy of change map is highly depended upon the algorithm used for threshold searching. To assess the proposed technique, experiments are carried out using three well known threshold algorithms (DFPS, T&E and 3×3 PKW) and compared their results with existing improved

samples from change magnitude imagery. It should also be noteworthy that all the threshold algorithms are implemented over topographically corrected mountainous region imagery because the pixels fallen under topographic effects such as shadow create problem in allocation of specific change category to a pixel. Therefore, topographic corrections become important to be implemented especially over mountainous region remotely sensed data to maintain the least commission SCVA (without fuzzy clustering) technique. The proposed technique is found to be imperious in terms of both accuracy as well as visual conformity as compare to improved SCVA. According to the findings, it is also concluded that incorporation of fuzzy logic and CVA based change detection model made a prominent and theoretically, well-justified algorithm especially in terms of threshold searching.

Major benefits of proposed technique are involved: (a) assigning multiple class categories to a pixel based on their belongingness; (b) ease in threshold procedures; and (c) make the full use of spatial information. The existing CVA based change detection algorithms does not provide solution in terms of detection of mixed pixels and conformity regarding threshold searching procedure. Further enhancements towards

Table 6 Accuracy assessment for different threshold determination techniques

Techniques	Categories	Reference Pixels	Classified pixels	Correct pixels	Incorrect pixels	PA	UA	Kc
DFPS with FMLC based CVA	Soil to snow	156	158	145	13	92.95	91.77	0.78
	Snow to mix	2	-	-	-	-	-	-
	Soil to mix	48	40	35	5	72.92	87.50	0.84
	Mix to snow	47	58	46	12	97.87	79.31	0.74
	Others	3	-	-	-	-	-	-
	Total pixels	256	256	226	30			
Overall accuracy = 88.28%, Kappa coefficient = 0.7881								
T&E with FMLC based CVA	Soil to snow	152	158	141	17	92.76	89.24	0.73
	Snow to mix	1	-	-	-	-	-	-
	Soil to mix	53	40	36	4	67.92	90	0.87
	Mix to snow	47	58	46	12	97.87	79.31	0.74
	Others	3	-	-	-	-	-	-
	Total pixels	256	256	223	33			
Overall accuracy = 87.11%, Kappa coefficient = 0.7696								
3×3 PKW with FMLC based CVA	Soil to snow	127	136	119	17	93.7	87.5	0.75
	Soil to mix	35	29	24	5	68.57	82.76	0.80
	Mix to snow	92	91	78	13	84.78	85.71	0.77
	Unclassified	2	-	-	-	-	-	-
	Total pixels	256	256	221	35			
Overall accuracy = 86.33%, Kappa coefficient = 0.7695								
DFPS with improved SCVA	Soil to snow	138	154	129	25	93.48	83.77	0.64
	Snow to mix	13	2	2	-	15.38	100	1
	Soil to mix	30	30	25	5	83.33	83.33	0.81
	Mix to snow	69	70	62	8	89.86	88.57	0.84
	Others	6	-	-	-	-	-	-
Total pixels	256	256	218	38				
Overall accuracy = 85.16%, Kappa coefficient = 0.7475								
Trial & Error with improved SCVA	Soil to snow	150	173	143	30	95.33	82.66	0.58
	Snow to mix	-	-	-	-	-	-	-
	Soil to mix	45	22	18	4	40	81.82	0.77
	Mix to snow	56	61	48	13	85.71	78.69	0.72
	Unclassified	5	-	-	-	-	-	-
	Total pixels	256	256	209	47			
Overall accuracy = 81.64%, Kappa coefficient = 0.6580								
3×3 PKW with improved SCVA	Soil to snow	136	152	130	22	95.59	85.53	0.69
	Soil to mix	36	21	18	3	50	85.71	0.83
	Mix to snow	81	83	65	18	80.25	78.31	0.68
	Others	3	-	-	-	-	-	-
	Total pixels	256	256	213	43			
Overall accuracy = 83.20%, Kappa coefficient = 0.70								

proposed technique may comprise the identification of mixed pixels by the integration of subpixel classification. Although selection of potential threshold is a topic of continuous

research so, some future pursuits could be focused on problem of threshold searching by using optimization methods.

Acknowledgement

The authors would like to express their gratitude to the anonymous referees and the editor for their constructive comments and valuable suggestions, that helped to significantly improve the earlier version of manuscript. We further

gratefully acknowledge NASA for providing the Moderate Resolution Imaging Spectroradiometer (MODIS) data and U.S. Geological Survey (USGS) for provision of ASTER Global DEM version 2 data.

References

- Allen TR, Kupfer JA (2000) Application of spherical statistics to change vector analysis of Landsat data: Southern Appalachian spruce-fir forests. *Remote Sensing of Environment* 74(3): 482-493. DOI: [10.1016/S0034-4257\(00\)00140-1](https://doi.org/10.1016/S0034-4257(00)00140-1)
- Baisantry M, Negi DS, Manocha OP (2012) Change vector analysis using enhanced PCA and inverse triangular function-based thresholding. *Defence Science Journal* 62(4): 236-242. DOI: [10.14429/dsj.62.1072](https://doi.org/10.14429/dsj.62.1072)
- Chen J, Gong, P, He C, et al. (2003) Landuse/ land-cover change detection using improved change-vector analysis. *Photogrammetric Engineering and Remote Sensing* 69(4): 369-379. DOI: [10.14358/PERS.69.4.369](https://doi.org/10.14358/PERS.69.4.369)
- Chen J, Chen X, Cui X et al. (2011) Change vector analysis in posterior probability space: a new technique for land cover change detection. *IEEE Geo-science and Remote Sensing Letters* 8(2): 317-321. DOI: [10.1109/LGRS.2010.2068537](https://doi.org/10.1109/LGRS.2010.2068537)
- He C, Zhao Y, Tian J, et al. (2013) Improving change vector analysis by cross-correlogram spectral matching for accurate detection of land-cover conversion. *International Journal of Remote Sensing* 34(4): 1127-1145. DOI: [10.1080/01431161.2012.718458](https://doi.org/10.1080/01431161.2012.718458)
- ERDAS (1999) ERDAS: Field Guide. ERDAS Inc., Atlanta, Georgia, p 671.
- Fung T, LeDrew E (1988) The determination of optimal threshold levels for change detection using various accuracy indices. *Photogrammetric Engineering & Remote Sensing* 54: 1449-1454.
- Foody GM, Atkinson PM (2002) Uncertainty in remote sensing and GIS, John Wiley & Sons. DOI: [10.1002/0470035269](https://doi.org/10.1002/0470035269)
- Johnson RD, Kasischke ES (1998) Change vector analysis: a technique for the multitemporal monitoring of land cover and condition. *International Journal of Remote Sensing* 19: 411-426. DOI: [10.1080/014311698216062](https://doi.org/10.1080/014311698216062)
- Kontoes CC (2008) Operational land cover change detection using change vector analysis. *International Journal of Remote Sensing* 29(16): 4757-4779. DOI: [10.1080/01431160801961367](https://doi.org/10.1080/01431160801961367)
- Lambin EF, Strahler AH (1994) Change-vector analysis in multi-temporal space: a tool to detect and categorize land-cover change processes using high temporal-resolution satellite data. *Remote Sensing of Environment* 48(2): 231-244. DOI: [10.1016/0034-4257\(94\)90144-9](https://doi.org/10.1016/0034-4257(94)90144-9)
- Lu D, Mausel P, Brondizio E, et al. (2004) Change detection techniques. *International Journal of Remote Sensing* 25(12): 2365-2407. DOI: [10.1080/0143116031000139863](https://doi.org/10.1080/0143116031000139863)
- Malila WA (1980) Change vector analysis: an approach for detecting forest changes with Landsat, In Proceedings of the 6th Annual Symposium on Machine Processing of Remotely Sensed Data, 3-6 June 1980, West Lafayette, IN (West Lafayette: Purdue University), 326-335.
- Mather PM (2004) Computer processing of remotely-sensed images: an introduction, Wiley, 2, Chichester.
- Melesse AM, Jordan JD (2002) A comparison of fuzzy vs. augmented-ISODATA classification algorithms for cloud-shadow discrimination from Landsat images. *Photogrammetric Engineering & Remote Sensing* 68: 905-911. DOI: [10.1080/0143116021000139863](https://doi.org/10.1080/0143116021000139863)
- Michalek JL, Wagner TW, Luczkovich JJ, et al. (1993) Multispectral change vector analysis for monitoring coastal marine environments. *Photogrammetric Engineering and Remote Sensing* 59: 381-384.
- Mishra VD, Sharma JK, Singh KK, et al. (2009a) Assessment of different topographic corrections in AWiFS satellite imagery of Himalaya terrain. *Journal of Earth System Sciences* 118(1): 11-26. DOI: [10.1007/s12040-009-0002-0](https://doi.org/10.1007/s12040-009-0002-0)
- Mishra VD, Sharma JK and Khanna R (2009b) Review of topographic analysis techniques for the western Himalaya using AWiFS and MODIS satellite imagery. *Annals of Glaciology* 51(54): 1-8. DOI: [10.3189/172756410791386526](https://doi.org/10.3189/172756410791386526)
- Mishra NS, Ghosh S, Ghosh A (2012) Fuzzy clustering algorithms incorporating local information for change detection in remotely sensed images. *Applied Soft Computing* 12: 2683-2692. DOI: [10.1016/j.asoc.2012.03.060](https://doi.org/10.1016/j.asoc.2012.03.060)
- Nackaerts K, Vaesen K, Muys B, et al. (2005) Comparative performance of a modified change vector analysis in forest change detection. *International Journal of Remote Sensing* 26(5): 839-852. DOI: [10.1080/0143116032000160462](https://doi.org/10.1080/0143116032000160462)
- Nichol J, Hang LK, Sing WM (2006) Empirical correction of low sun angle images in steeply sloping terrain: a slope matching technique. *International Journal of Remote Sensing* 27(3-4): 629-635. DOI: [10.1080/02781070500293414](https://doi.org/10.1080/02781070500293414)
- Sharma JK, Mishra VD, Khanna R (2013) Impact of topography on accuracy of land cover spectral change vector analysis using AWiFS in Western Himalaya. *Journal of the Indian Society of Remote Sensing* 41(2): 223-235. DOI: [10.1007/s12524-011-0180-5](https://doi.org/10.1007/s12524-011-0180-5)
- Silva PG, Santos JR, Shimabukuro YE, et al. (2003) Change vector analysis technique to monitor selective logging activities in Amazon. *IEEE Proceedings International Geoscience and Remote Sensing Symposium*, 2580-2582. DOI: [10.1109/IGARSS.2003.1294515](https://doi.org/10.1109/IGARSS.2003.1294515)
- Singh S, Sharma JK, Mishra VD (2011) Comparison of different topographic correction methods using AWiFS satellite data. *International Journal of Advanced Engineering Sciences and Technologies* 7(1):85-91.
- Singh S, and Talwar R (2014) A comparative study on change vector analysis based change detection techniques. *SADHANA-Academy Proceedings in Engineering Sciences* 39(6): 1311-1331. DOI: [10.1007/s12046-014-0286-x](https://doi.org/10.1007/s12046-014-0286-x)
- Singh S, Talwar R (2015a) Assessment of different CVA based change detection techniques using MODIS dataset. *MAUSAM Journal* 66(1): 77-86.
- Singh S, Talwar R (2015b) Performance analysis of different threshold determination techniques for change vector analysis. *Journal of Geological Society of India* 86: 52-58. DOI: [10.1007/s12594-015-0280-x](https://doi.org/10.1007/s12594-015-0280-x)
- Singh S, Talwar R (2016) An intercomparison of different topography effects on discrimination performance of fuzzy change vector analysis algorithm. *Meteorology Atmospheric Physics* 128(6): 1-14. DOI: [10.1007/s00703-016-0494-5](https://doi.org/10.1007/s00703-016-0494-5)
- Thonfeld F, Hannes F, Braunc M, et al. (2016) Robust Change Vector Analysis (RCVA) for multi-sensor very high resolution optical satellite data. *International Journal of Applied Earth Observation and Geoinformation* 50: 131-140. DOI: [10.1016/j.jag.2016.03.009](https://doi.org/10.1016/j.jag.2016.03.009)
- Varshney A, Arora MK, Ghosh JK (2012) Median change vector analysis algorithm for land-use land-cover change detection from remote-sensing data. *Remote Sensing Letters* 3(7): 605-614. DOI: [10.1080/01431161.2011.648281](https://doi.org/10.1080/01431161.2011.648281)
- Zhang J, Foody GM (1998) A fuzzy classification of sub-urban land cover from remotely sensed imagery. *International Journal of Remote Sensing* 9(14): 2721-2738. DOI: [10.1080/01431169821447](https://doi.org/10.1080/01431169821447)